

Nanophase Segregation Drives Heterogeneous Dynamics in Amphiphilic PLMA-*b*-POEGMA Block-Copolymers with Densely Grafted Architecture

Achilleas Pipertzis,* Athanasios Skandalis, Stergios Pispas,* and George Floudas

The self-assembly and dynamics of amphiphilic diblock copolymers composed of densely grafted poly(oligo ethylene glycol methacrylate) (POEGMA) and poly(lauryl methacrylate) (PLMA) by means of calorimetry, small-angle X-ray scattering (SAXS), and dielectric spectroscopy are investigated. It is reported that the inherent immiscibility between the parent homopolymers, combined with the increased molar mass, results in strong segregation, maintained up to elevated temperatures (i.e., $T = 423$ K). SAXS reveals that well-separated POEGMA and PLMA domains self-assemble into spheres with bicontinuous cubic packing and in lamellar nanostructure in copolymers with respective compositions of 16 and 52 wt.% PLMA. This strong segregation enables the weak crystallization/melting of the short ethylene glycol chains. Additionally, molecular dynamics are investigated through isothermal dielectric and calorimetry measurements. The segmental dynamics (i.e., T_g -related) of POEGMA and PLMA closely resemble that found in respective homopolymers, implying heterogeneous dynamics. In the glassy state, the local motions of the POEGMA side chains predominantly govern the observed secondary processes in the copolymers. The results on the *heterogeneous dynamics* in the current *amphiphilic* diblock copolymers with the densely grafted architecture are compared and contrasted with copolymers having a bottle-brush architecture lacking the amphiphilic nature.

1. Introduction

Block copolymers can self-assemble into a variety of nano-segregated morphologies, amalgamating the inherent properties of each block into a single material.^[1] In their dry state, the segregation strength is determined by the product χN , where χ is the Flory-Huggins interaction parameter between A and B blocks, and N is the total degree of polymerization.^[1,2] Different nanostructures can be obtained by changing the composition, the degree of segregation, and the block architecture (i.e., linear vs densely grafted). Expectedly, the compatibility and the local segregation strength among the constituents can affect the molecular dynamics of the copolymers.

Amphiphilic block copolymers (AmBCs) are composed of two or more macromolecular chains covalently linked, each possessing different levels of hydrophobicity. In solution, these copolymers serve as ideal candidates for encapsulating and delivering hydrophobic drugs and imaging agents within their hydrophilic cores.^[3,4] Extensively studied in recent

years, amphiphilic block copolymers (AmBCs) demonstrate the capability to self-assemble at the nanoscale into spherical or cylindrical micelles and vesicles (polymersomes) when placed in proper solvents.^[5,6] In this case, the hydrophobic polymer chains form the core, while the hydrophilic chains form the corona. Moreover, AmBCs can exhibit phase separation in semi-dilute aqueous solutions under varying environmental conditions such as temperature, pH, and concentration.^[6,7]

Recently, AmBCs with a densely grafted macromolecular architecture have been successfully synthesized using a reversible addition-fragmentation chain transfer (RAFT) polymerization process. These copolymers consist of poly(lauryl methacrylate) (PLMA) with poly(oligo ethylene glycol methacrylate) (POEGMA), yielding different hydrophilic/hydrophobic block ratios and well-defined molecular characteristics.^[3,4] Studies on the self-assembly have revealed the formation of micelles with large aggregation numbers and soft cores, as confirmed by light scattering and TEM techniques. Utilization of PLMA-*b*-POEGMA micelles as nanocarriers has shown promise for the encapsulation of magnetic nanoparticles (NPs), and both NPs

A. Pipertzis, G. Floudas
 Department of Physics
 University of Ioannina
 Ioannina 45110, Greece
 E-mail: achilleas.pipertzis@chalmers.se

A. Skandalis, S. Pispas
 Theoretical and Physical Chemistry Institute
 National Hellenic Research Foundation
 48 Vassileos Constantinou Ave., Athens 11635, Greece
 E-mail: pispas@eie.gr

G. Floudas
 Max Planck Institute for Polymer Research
 Ackermannweg 10, 55128 Mainz, Germany

 The ORCID identification number(s) for the author(s) of this article can be found under <https://doi.org/10.1002/macp.202400180>

© 2024 The Author(s). Macromolecular Chemistry and Physics published by Wiley-VCH GmbH. This is an open access article under the terms of the [Creative Commons Attribution-NonCommercial](https://creativecommons.org/licenses/by-nc/4.0/) License, which permits use, distribution and reproduction in any medium, provided the original work is properly cited and is not used for commercial purposes.

DOI: 10.1002/macp.202400180

and a model hydrophobic drug (indomethacin), leading to improved stability and biocompatibility.^[4]

Well-known as *smart* polymer, POEGMA emerges as a promising comb-like and thermoresponsive polymer (i.e., low critical solution temperature to water) for biomedical and energy storage applications, the latter following doping with Li salt. Its biological significance arises from its biocompatibility and non-immunogenic nature. For energy applications, the biodegradable polymer's densely grafted architecture, coupled with short ethylene glycol side groups, suppresses crystallinity and enhances segmental mobility, thereby engineering high ionic conductivities, that motivated studies related to solid polymer electrolytes.^[8] Recent investigations of the molecular dynamics of POEGMA homopolymers in the dry state have unveiled the presence of two secondary processes, reflecting local motions of the hydrophilic side chain into the glassy state.^[9] These processes are followed by a segmental T_g -related process.^[9]

Another important class of comb-like polymers encompasses poly(*n*-alkylmethacrylates).^[10–15] Studies have demonstrated the ability to shift T_g -related dynamics by over 150 K when transitioning from the first member of the series, poly(methyl methacrylate) (PMMA) to PLMA (bearing 12 methylene units). Employing a combination of dielectric and dynamic depolarized light scattering (DLS) experiments, it was evidenced that the primary and secondary relaxations are associated with the ester side group, possessing most of the dipole moment and optical anisotropy, respectively.^[10] In methacrylates with long side groups, a coupling between the α and the slow β processes was evident.^[10]

Molecular dynamics studies on certain AmBCs in their dry state have been conducted.^[16] Specifically, Karatzas et al.^[16] investigated the relaxation dynamics of new thermoresponsive amphiphilic poly(hydroxyl propyl methacrylate) -*b*- poly(oligo ethylene glycol methacrylate) (PHPMA-*b*-POEGMA) diblock copolymers through calorimetry (DSC) and dielectric spectroscopy (BDS).^[16] It was revealed that the single glass temperature (T_g) and the associated segmental dynamics were predominantly governed by the POEGMA ($T_g \approx 213$ K) for PHPMA content up to ≈ 50 wt.%. Only at higher PHPMA content there was a significant increase in T_g suggesting the plasticization of the PHPMA segmental dynamics.^[16] Moreover, Mierzwa et al.^[17] studied the relaxation dynamics in densely grafted systems (i.e., known as “hairy rods”), composed of a stiff backbone and flexible short ethylene oxide (EO) side chains, signifying the importance of densely grafted architecture for examining the effect of confinement on molecular dynamics, by employing dielectric and Nuclear Magnetic Resonance (NMR) measurements.^[17] It was evidenced that mainly the segmental relaxation was affected upon confinement.^[17] To date, there exists a gap in the literature regarding the investigation of nanophase separation and molecular dynamics in PLMA-*b*-POEGMA copolymers in their dry state. This study aims to address this gap.

Herein, we investigate the thermodynamics, structural properties, and molecular dynamics in AmBCs composed of one hydrophobic (PLMA) block and one hydrophilic (POEGMA) block. By employing SAXS, dielectric, and calorimetric measurements, we report strong nanophase segregation that drives the heterogeneous dynamics between the two blocks. The results are compared with copolymers having a bottle-brush architecture but without the amphiphilic nature.

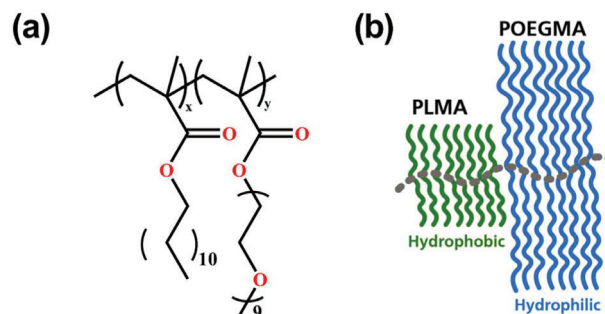


Figure 1. a) Chemical structure of the amphiphilic PLMA-*b*-POEGMA diblock copolymers. b) Schematic representation of their grafted architecture.

2. Experimental Section

2.1. Synthesis of PLMA-*b*-POEGMA

The block copolymers were prepared by RAFT polymerization, as described elsewhere.^[3,4] RAFT polymerization stands out as a versatile technique extensively utilized for synthesizing well-defined amphiphilic block copolymers with densely grafted architecture, offering advantages such as control over molar mass (M_w) and polydispersity values close to unity, alongside compatibility with a wide array of monomers.^[18–20] The chemical structure of the investigated AmBCs is depicted in **Figure 1**, along with a schematic representation depicting their densely grafted macromolecular architecture and the different side group lengths of the two blocks.

The molecular characteristics of the studied AmBCs and their respective homopolymers are provided in **Table 1**.

2.2. Differential Scanning Calorimetry

For the investigation of thermodynamics of the amphiphilic PLMA-*b*-POEGMA copolymers and their respective homopolymers, a Q2000 Differential Scanning Calorimetry (DSC) setup (TA Instruments) was utilized. The instrument was calibrated to optimize performance within the designated temperature range and heating/cooling rate. Calibration procedures included baseline calibration to determine time constants and capacitances of the sample and the reference sensor using a sapphire standard. Subsequently, an indium standard ($\Delta H = 28.71$ J g⁻¹, $T_m = 428.8$ K, with a heating rate of 10 K min⁻¹) was employed for enthalpy and transition temperature calibration. Following indium calibration, a baseline measurement was made. The temperature protocol involved an initial cycle of cooling and heating at a rate

Table 1. Molecular Characteristics of PLMA-*b*-POEGMA Copolymers and Corresponding Homopolymers.

Sample code	M_w [g mol ⁻¹] ^{a)}	\bar{D} ^{a)}	x	y	wt.% PLMA ^{b)}
POEGMA	17200	1.2	–	36	0
PLMA ₁₆ - <i>b</i> -POEGMA ₈₄	33000	1.3	21	58	16
PLMA ₅₂ - <i>b</i> -POEGMA ₄₈	11700	1.18	24	12	52
PLMA	6900	1.09	27	–	100

^{a)} Determined via SEC; ^{b)} Determined via ¹H-NMR. Subscripts in sample names denote wt.% of each block.

of 10 K min⁻¹ to erase the thermal history, followed by a second cycle within the same temperature range (173 to 423 K) with the same rate. In addition, a slow cooling/heating rate of 2 K min⁻¹ was employed to facilitate the comparison with dielectric spectroscopy measurements.

Temperature-modulated DSC measurements were conducted in the AmBC with symmetric composition for identifying the T_g^{PLMA} , that is overlapped from the cold-crystallization of the POEGMA side groups (see below). TM-DSC enables the separation of overlapping phenomena, through the reversing signal of heat capacity.^[21,22] Measurements were performed within the temperature range from 183 to 273 K. In TM-DSC a low-frequency sinusoidal perturbation is summarized to the standard DSC profile, according to $T = T_0 + \beta t + A_T \sin(\omega t)$, where β is the linear cooling/heating rate, t the time, A_T the amplitude, and ω the angular frequency. An amplitude of 1 K and two periods of modulation (i.e., 200 and 100 s) with respective heating rates of 1 and 2 K min⁻¹ have been employed.

2.3. Small-Angle X-Ray Scattering (SAXS)

SAXS measurements were conducted using Cu Ka radiation (RigakuMicroMax 007 X-ray generator, Osmic Confocal Max-Flux curved multilayer optics). Scattering patterns were captured on a Mar345 image plate at a sample-to-detector distance of 2.11 m. Intensity distributions from the recorded patterns were analyzed as a function of the modulus of the scattering vector, q ($q = (4\pi/\lambda) \sin(2\theta/2)$, where, λ , is the wavelength $\lambda = 0.154184$ nm and 2θ is the scattering angle). Temperature-dependent SAXS measurements were conducted in the temperature range from 293 to 433 K upon heating in increments of 10 K for PLMA₁₆-*b*-POEGMA₈₄ and from 293 to 323 K for PLMA₅₂-*b*-POEGMA₄₈. Each measurement lasted for one hour following an hour of equilibration at each temperature.

2.4. Dielectric Spectroscopy (DS)

DS measurements were carried out using a Novocontrol Alpha frequency analyzer. The temperature stability was controlled using a nitrogen gas Quatro cryosystem, with a stability of ± 0.05 °C. The temperature protocol involved measurements from 173 to 323 K in steps of 5 K and for frequencies ranging from 10⁻² to 10⁷ Hz, under atmospheric pressure. The dielectric cell comprised two electrodes, each 20 mm in diameter, with the sample held at a thickness of 100 μ m by Teflon spacers. Samples were prepared as melts under vacuum by pressing the electrodes to achieve the desired spacer thickness.

The complex dielectric permittivity $\epsilon^* = \epsilon' - i\epsilon''$, where ϵ' is the real and ϵ'' is the imaginary part, was obtained as a function of frequency, ω , temperature, T , and pressure, P , i.e., $\epsilon^*(T, P, \omega)$.^[23,24] The determination of relaxation dynamics was made using the empirical equation of Havriliak and Negami (HN) with an additional conductivity contribution:

$$\epsilon_{HN}^*(\omega, T, P) = \epsilon_\infty(T, P) + \sum_{j=1}^3 \frac{\Delta\epsilon(T, P)}{\left[1 + \left(i\omega \cdot \tau_{HN_j}(T, P)\right)^{m_j}\right]^{n_j}} + \frac{\sigma_0(T, P)}{i\epsilon_f\omega} \quad (1)$$

where, $\epsilon_\infty(T, P)$ is the high-frequency permittivity, $\tau_{HN}(T, P)$ is the characteristic relaxation time in this equation, $\Delta\epsilon(T, P) = \epsilon_0(T, P) - \epsilon_\infty(T, P)$ is the relaxation strength, m , n (with limits $0.2 < m, mn \leq 1$) describe, respectively, the symmetrical and asymmetrical broadening of the distribution of relaxation times, σ_0 is the dc conductivity, and ϵ_f is the permittivity of free space. From τ_{HN} , the relaxation time at maximum loss, τ_{max} , is obtained analytically as follows:^[25]

$$\tau_{max} = \tau_{HN} \sin^{-1/m} \left(\frac{\pi m}{2(1+n)} \right) \sin^{1/m} \left(\frac{\pi mn}{2(1+n)} \right) \quad (2)$$

For analyzing the dynamic behavior, the ϵ'' values are used at every temperature along with the derivative of dielectric permittivity, for suppressing the conductivity contribution. Moreover, the real part of complex conductivity, σ' to determine the values of dc-conductivity is employed.

3. Results and Discussion

3.1. Thermodynamics

Comprehensive understanding of the thermodynamic transitions in amphiphilic comb-like block copolymers can be attained through a combination of thermodynamic (DSC) and dynamic (DS) measurements. The thermograms of the investigated PLMA-*b*-POEGMA copolymers and their respective homopolymers are shown in **Figure 2a**.

Several studies^[10,11] have documented that the dominant factor governing segmental dynamics and the associated T_g in comb-like polymers is the length of the side groups. As depicted in **Figure 2**, the POEGMA and PLMA homopolymers exhibit respective liquid-to-glass temperatures at 213 and 232 K, consistent with literature reports.^[9,10] Hence, the T_g^{POEGMA} is lower by about 20 K compared to T_g^{PLMA} , indicating a stronger plasticization effect for POEGMA. Moreover, the POEGMA homopolymer displays a weak cold-crystallization followed by melting, at higher temperatures, indicating the crystallization and melting of side groups that is possible here because of nanophase separation.^[3,26–27] It has been confirmed that crystallization of the polymer network can be observed for POEGMA side chain lengths longer than 7 ethylene-oxide units.^[27]

Concerning the AmBCs, the conventional DSC thermograms reflect the thermodynamic features of the POEGMA homopolymer. It is worth noting that the T_g^{POEGMA} is ≈ 2 –5 K lower than that found in POEGMA homopolymer, indicating possible confinement effects.^[17,28] Furthermore, the weak cold-crystallization and melting of the short ethylene glycol side chains can be observed for both AmBCs compositions suggesting the presence of well-separated domains, as further demonstrated below with the help of SAXS. The results are provided in **Table 2**. The observed low enthalpy of melting values of POEGMA crystallization/melting are in accordance with literature.^[27] However, since the cold-crystallization peak and the T_g^{PLMA} occur within the same temperature range, and thus TM-DSC measurements are required to accurately identify the vitrification temperature of the PLMA segments.

The reversing heat capacity trace shows two clear steps: one at 211 K associated with the vitrification of amorphous POEGMA

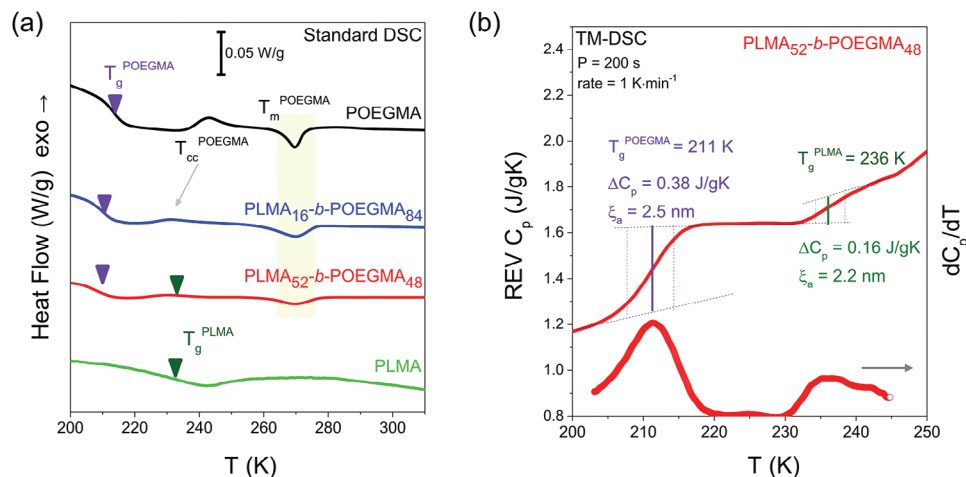


Figure 2. a) Standard DSC thermograms of POEGMA (black), PLMA₁₆-*b*-POEGMA₈₄ (blue), PLMA₅₂-*b*-POEGMA₄₈ (red), and PLMA (green) upon heating with a rate of 2 K min⁻¹. Traces are shifted vertically for clarity. The vertical purple and green arrows indicate the liquid-to-glass temperatures of POEGMA and PLMA, respectively. b) The TM-DSC trace for the amphiphilic diblock copolymer with 52 wt. % of PLMA shows two glass temperatures.

segments and another at 236 K attributed to the vitrification of PLMA segments (see Figure 2b). At this point, it needs to be mentioned that the presence of two T_g s does not necessarily indicate immiscibility between the two blocks.^[29] A definitive answer requires a structural investigation (see SAXS below). The change of heat capacity at T_g , ΔC_p , for the T_g^{POEGMA} is much stronger (three-fold) compared to that of T_g^{PLMA} , reflecting the degrees of freedom and the distinctly different nature of the two homopolymers. From the TM-DSC thermogram, the characteristic length scale, ξ_a , associated with the two T_g s can also be extracted. It is related to the length scale of cooperatively rearranging regions (CRR), as introduced by Adam and Gibbs,^[30] defined as the smallest volume element that can change configuration independently of its environment. Specifically, ξ_a can be calculated by employing the Donth model using the following equation:^[31]

$$\xi_a = \left(\frac{3k_B T_g^2 \Delta(1/C_p)}{4\pi\rho(\delta T)^2} \right)^{1/3} \quad (3)$$

where, k_B is the Boltzmann constant, ρ is the mass density, $\Delta(1/C_p) = 1/C_p^{\text{glass}} - 1/C_p^{\text{liquid}}$, calculated at T_g , and $\delta T = \Delta T/2.5$, is the mean temperature fluctuation of CRR. Accordingly, the corresponding cooperative rearranging regions have correlation lengths of 2.5 and 2.2 nm for the lower and higher T_g s, respectively. For the PLMA₁₆-*b*-POEGMA₈₄ copolymer, the T_g^{PLMA} is ab-

sent from the TM-DSC thermograms, reflecting mainly sensitivity issues. Additional understanding of the dynamics related to T_g and the impact of immiscibility between the two blocks on the molecular dynamics of the copolymers can be gained through dielectric measurements performed as a function of temperature, elaborated upon below.

Isochronal dielectric spectroscopy measurements serve as a complementary technique for obtaining the characteristics of the phase “transitions”. The temperature dependence of dielectric permittivity, ϵ' , and the first derivative of dielectric permittivity with respect to temperature are presented in Figure 3. It is well-documented in literature that the latter representation provides information about the exact temperature of phase transitions.^[32]

There is an abrupt change of dielectric permittivity on heating, reflecting the cold crystallization and subsequent melting of POEGMA. Moreover, there is a hysteresis between cooling and heating, characteristic of first-order transitions. The corresponding transitions closely align with those obtained from DSC, as evident from the phase diagram in Figure 4a.

POEGMA homopolymer exhibits higher values of dielectric permittivity into the different regions (glassy, crystalline, melting state) compared to the PLMA homopolymer, reflecting the polarity of the side groups. For the AmBCs, the inverse dielectric permittivity is proportional to the weight fraction of the PLMA described by the following mixing rule: $(1/\epsilon'_{\text{copolymer}} = (1 - \text{wt}_{\text{PLMA}})(1/\epsilon'_{\text{POEGMA}}) + \text{wt}_{\text{PLMA}}(1/\epsilon'_{\text{PLMA}}))$, for a two-phase system, implying incompatibility between the two blocks (see Figure 4b). At this point, the self-assembly and the segregation strength between the two blocks needs to be elucidated by X-rays.

3.2. Copolymer Morphology

Precise information about the degree of segregation between the PLMA and POEGMA blocks can be obtained by X-ray measurements. The SAXS patterns of the amphiphilic PLMA-*b*-POEGMA copolymers at a fixed temperature (i.e., $T = 293$ K) are provided in Figure 5.

Table 2. Calorimetric Data of Glass, Cold-Crystallization, and Melting Temperatures along with the Enthalpy of Melting.

Sample code	T_g^{POEGMA} [K]	T_g^{PLMA} [K]	T_{cc} [K]	T_m [K]	ΔH_m [J g ⁻¹]
POEGMA	213 ± 1	–	243 ± 1	270 ± 1	6 ± 1
PLMA ₁₆ - <i>b</i> -POEGMA ₈₄	208 ± 1	–	231 ± 1	269 ± 1	5 ± 2
PLMA ₅₂ - <i>b</i> -POEGMA ₄₈	211 ± 1	236 ± 3	229 ± 1	270 ± 1	3 ± 1
PLMA	–	232 ± 5	–	–	–

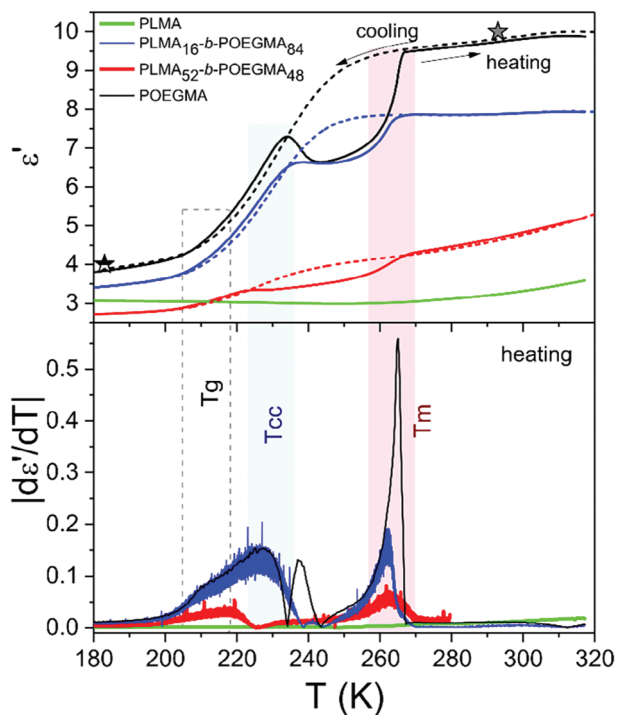


Figure 3. (Top) Temperature dependence of dielectric permittivity, ϵ' for POEGMA (black), PLMA₁₆-*b*-POEGMA₈₄ (blue), PLMA₅₂-*b*-POEGMA₄₈ (red), and PLMA (green), upon cooling (dashed lines) and subsequent heating (solid lines), both with a rate of 2 K min⁻¹. Measurements refer to a frequency of 0.1 MHz. (Bottom) First derivative of dielectric permittivity with respect to temperature, during heating. The star symbols indicate the dielectric permittivity values reported in ref. [33] (filled star) and ref. [16] (semi-filled star), for the POEGMA homopolymer.

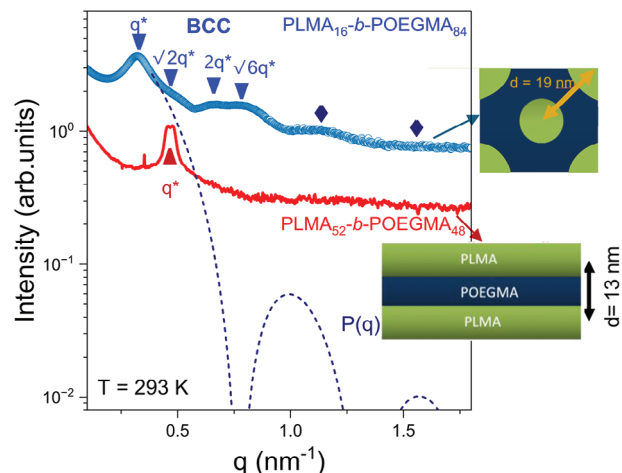


Figure 5. a) SAXS patterns for PLMA₁₆-*b*-POEGMA₈₄ (blue symbols) and PLMA₅₂-*b*-POEGMA₄₈ (red line) copolymers, at 293 K. The dashed blue line represents fit to Equation (5) for the PLMA₁₆-*b*-POEGMA₈₄ copolymer. Arrows and rhombi indicate the structure and form factor peaks, respectively. The pattern for PLMA₅₂-*b*-POEGMA₄₈ is shifted vertically for clarity. Schematic representations of the body-centered cubic and lamellar morphologies are also depicted.

Starting from the PLMA₁₆-*b*-POEGMA₈₄, the scattered intensity can be expressed as:

$$I(q) \sim K \cdot P(q) \cdot S(q) \quad (4)$$

where, K is a scaling factor, $S(q)$, is the structure factor and, $P(q)$, is the form factor. The latter factor reflects the scattering coming from the shape of the particles. The broad features at higher

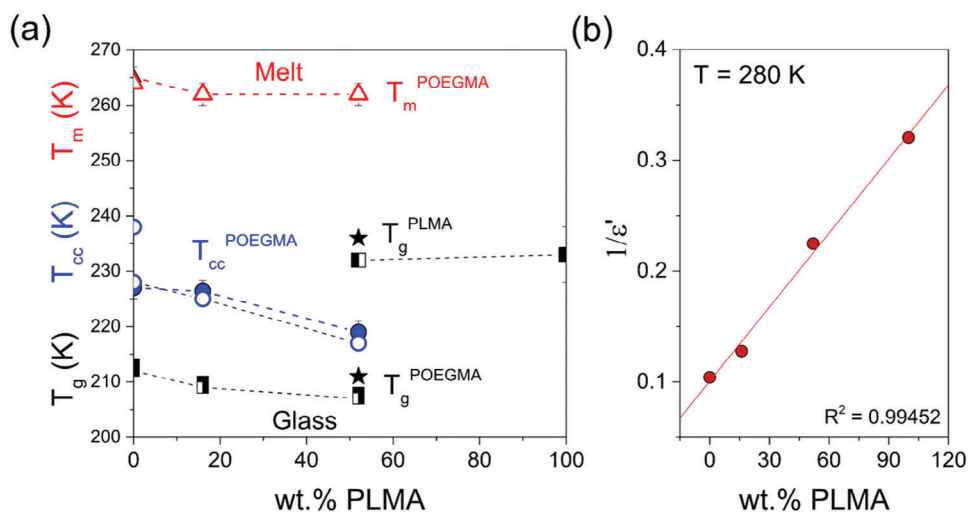


Figure 4. a) Phase diagram depicting the melting (red triangles), cold-crystallization (blue circles), and glass (black squares and stars) temperatures as a function of the PLMA weight fraction, upon heating. Filled symbols are extracted from thermodynamic measurements (DSC) with a rate of 2 K min⁻¹. Open symbols are obtained from isochronal dielectric measurements at a frequency of 0.1 MHz and a rate of 2 K min⁻¹. The T_g values are obtained from DSC (filled squares), TM-DSC (stars), and isothermal dielectric spectroscopy (semi-filled squares) measurements at a relaxation time of 100 s. b) Inverse dielectric permittivity as a function of the PLMA content at $T = 280$ K (melt). The R^2 value of the linear fitting is included.

q -values can be simulated by the form factor of homogeneous spheres with a radius R that is given by:^[34]

$$P(q) = u_0^2 \left[\frac{3}{(qR)^3} [\sin(qR) - qR\cos(qR)] \right]^2 \quad (5)$$

where u_0 is the sphere volume. The simulation of the experimental scattering curve with Equation (5) is depicted in Figure 5. According to the form factor, the first minima is developed at $qR = 4.484$.^[34] By employing the latter position, a radius of PLMA spheres equal to $R \approx 5.8$ nm can be extracted.

In turn, the lower- q Bragg reflections arise from the structure factor, $S(q)$, that are associated with the spatial distribution of the scattering particles (spheres). From the position of the first maxima of $S(q)$, the inter-sphere distance (inter-particle interference) can be obtained. Specifically, the PLMA₁₆-*b*-POEGMA₈₄ display a peak at $q^* \approx 0.323$ nm⁻¹, that corresponds to a periodicity of $d = 2\pi/q^* \approx 19$ nm. Additional higher-order Bragg reflections with relative positions 1:2^{1/2}:2:6^{1/2}, suggesting PLMA spheres organized in a body-centered cubic lattice or in a simple cubic lattice.^[1] The presence of higher-order peaks imply a long-range order. As depicted in Figure S1 (Supporting Information), even at elevated temperatures (i.e., $T = 423$ K), the strong nanophase separation and long-range order is maintained, reflecting strong immiscibility between the two blocks.

Conversely, the PLMA₅₂-*b*-POEGMA₄₈ exhibits only a peak at $q^* \approx 0.472$ nm⁻¹, suggesting weaker segregation between the two blocks and lamellar formation with a thickness of $d \approx 13$ nm, at 293 K. The increased segregation strength/domain spacing in the PLMA₁₆-*b*-POEGMA₈₄ is in line with its higher molar mass (see “Experimental” section). Overall, AmBCs based on PLMA and POEGMA exhibit strong nanophase separation originating from their different interactions (hydrophilic/hydrophobic). A pertinent question here is how nanophase separation influences the molecular dynamics in the AmBCs.

3.3. Relaxation Dynamics

To address this point and obtain quantitative insight about the molecular dynamics in AmBCs, isothermal dielectric measurements were carried out across a wide temperature and frequency range. The relaxation dynamics of POEGMA and PLMA homopolymers are well-studied in literature and detailed in the Supporting Information with respect to Figures S2 and S3 (Supporting Information).^[9,10] Concerning the AmBCs, the dielectric curves of the copolymers with 52 and 16 wt.% of PLMA are presented in Figure 6 and Figure S4 (Supporting Information), respectively.

PLMA₅₂-*b*-POEGMA₄₈ exhibits five active dielectric processes into the experimental window, termed as; γ -, β_{POEGMA} -, α_{POEGMA} -, $\alpha\beta_{\text{PLMA}}$ - and σ_{POEGMA} -process, whose molecular origin is partly described by the name and would be elucidated below. The σ_{POEGMA} -process is exclusively evident in the derivative of dielectric permittivity. On the other hand, as shown in Figure S4 (Supporting Information), the α_{PLMA} is absent in the PLMA₁₆-*b*-POEGMA₈₄ copolymer, due to the low PLMA content, in line with the absence of a detectable PLMA T_g in calorimetry.

The T -dependence of the relaxation times at the maximum loss for all dielectrically active processes, for the two different copoly-

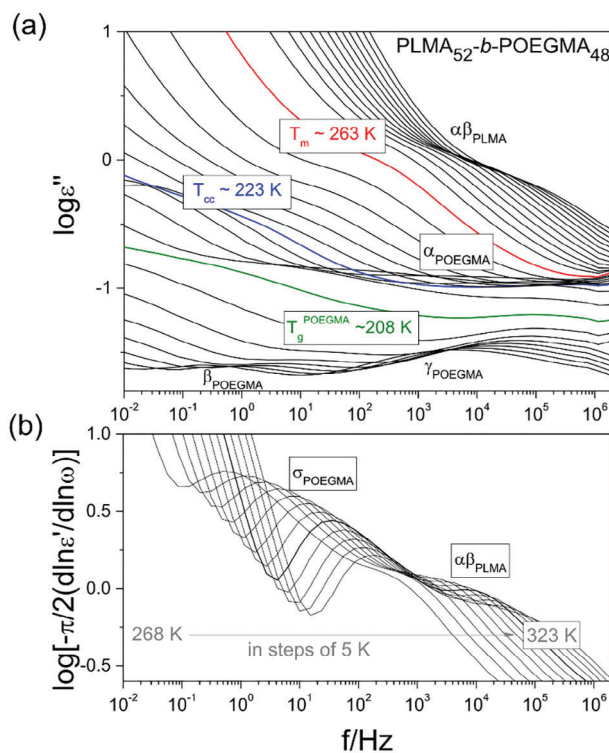


Figure 6. a) Dielectric loss curves for the PLMA₅₂-*b*-POEGMA₄₈ amphiphilic copolymer, at the investigated temperature range from 173 to 323 K in steps of 5 K. The glass temperature and the first-order transitions of POEGMA, observed in calorimetry, are indicated. b) Derivative of dielectric permittivity representation for suppressing the conductivity contribution, at higher temperatures; from 268 to 323 K, in increments of 5 K, upon heating.

mer compositions along with the respective homopolymers can be discussed with the help of Figure 7. The figure includes DSC and TM-DSC data, depicting the calorimetric T_g s.

Starting from lower temperatures, the γ and β_{POEGMA} processes exhibit a distribution of relaxation times reminiscent with that found in the POEGMA homopolymer, as depicted in Figure S5 (Supporting Information). The secondary processes exhibit an Arrhenius temperature dependence as:

$$\tau_{max} = \tau_0 \exp\left(\frac{E_a}{RT}\right) \quad (6)$$

where, τ_0 is the relaxation time in the limit of very high temperatures, and E_a is the activation energy. As listed in Table 3, the activation energy of the γ processes is reminiscent of that of POEGMA homopolymer. Hence, its molecular origin is ascribed to twisted motions of the EO side chains. The γ_{POEGMA} processes becomes slightly faster by decreasing the POEGMA content. Additionally, the β_{POEGMA} processes exhibit similar activation energies with that found in POEGMA homopolymer. There are three possible scenarios for its molecular origin: i) local motions of the hydrophilic part of the OEGMA chains, triggered by the presence of water molecules, ii) cooperative motions of the side group, assigned to the JG β -process, or iii) relaxation of ethylene oxide segments confined into the restricted amorphous phase.^[9,35,36] Tak-

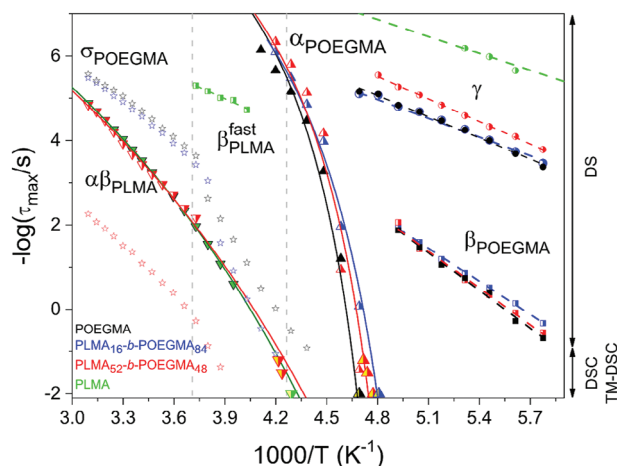


Figure 7. Relaxation times as a function of inverse temperature depicting the α_{PLMA} (down-triangles), β_{POEGMA} (squares), γ (circles), α_{POEGMA} (up-triangles), β_{PLMA} (semi-filled squares), σ_{POEGMA} (stars) and $\alpha\beta_{\text{PLMA}}$ (down-triangles) process, for the POEGMA (black), PLMA₁₆-*b*-POEGMA₈₄ (blue), PLMA₅₂-*b*-POEGMA₄₈ (red) and PLMA (green). All relaxation times were obtained on heating. The solid and dashed lines represent fits to VFT and Arrhenius equations, respectively. The symbols in yellow are extracted from TM-DSC measurements. The grey vertical dashed lines indicate the first-order transitions, observed in DSC and in the isochronal dielectric measurements.

ing into account the low hydration level of the samples (i.e., dried samples) and the distinctly low degrees of crystallinity along with the slower times compared to γ process, the second scenario is more plausible.

At higher temperatures, both the α_{POEGMA} and $\alpha\beta_{\text{PLMA}}$ processes conform to the Vogel–Fulcher–Tammann (VFT) dependence as:

$$\tau_{\text{max}} = \tau_0^{\#} \exp\left(\frac{B}{T - T_0}\right) \quad (7)$$

where, $\tau_0^{\#}$ is the relaxation time at very high temperatures and attains values in the order of picoseconds, B , is the activation parameter, and T_0 , is the "ideal" glass temperature located below

the conventional T_g , dielectrically defined at 100 s. The VFT and Arrhenius parameters of the dielectrically active processes, along with the values of the observed T_g s are provided in Table 3.

The α_{POEGMA} and α_{PLMA} processes are associated with the segmental relaxation of POEGMA and PLMA segments, as clearly evidenced in Figure 7. Notably, they are coupled with the segmental relaxation of POEGMA and PLMA homopolymers, respectively, implying a strong immiscibility and local segregation between the two blocks. It implies *heterogeneous dynamics* in AmBCs and confirms the presence of nearly pure POEGMA and PLMA domains (Figure 5). The calorimetric data were included in the fitting procedure of the two segmental processes. Remarkably, the segmental relaxation of POEGMA slightly speeds-up compared to the POEGMA homopolymer, in AmBCs, reflecting confinement effects, as discussed in SI with respect to Figures S6 and S7 (Supporting Information).^[17,28]

To quantify and compare the temperature dependence of the α_{POEGMA} and $\alpha\beta_{\text{PLMA}}$ relaxation times in the vicinity of the respective T_g s, we employ the steepness index (fragility), m . The steepness index can be calculated as $m^* = BT_g/[2.303(T_g - T_0)^2]$,^[37] or can be extracted from the slope at T_g in the fragility plot (see Figure 8). The extracted values are given in Table 3 and in Figure 8b. Both homopolymers and copolymers, display fragility values that are five-fold higher as compared to $\alpha\beta_{\text{PLMA}}$, verifying the inherently fragile and strong nature of POEGMA and PLMA segments, respectively. As extensively documented in the literature, in poly(*n*-methacrylates) the fragility decreases with increasing the side group length, implying a change from a "fragile" to a "strong" liquid as side group lengthens.^[10,11] The extracted fragilities for the segmental relaxation of POEGMA herein are close to the ones found for PEG.^[38]

The results from the present study can be compared with the segmental dynamics in model bottlebrush polymers consisting of poly(2-bromoisobutyryloxyethyl methacrylate) (PBiBEM) backbone and grafted *n*-butyl acrylate (PBA) chains.^[39] In the latter system the PBA segmental dynamics were slowed-down, whereas the backbone dynamics were plasticized by the side chains. Overall, the bottle-brush architecture was found to impart *dynamic homogeneity* to the backbone and side-chain dynamics. The situation in the present copolymers is very dif-

Table 3. Summary of VFT Parameters, Dielectric Glass Temperature and Fragility for the Investigated Grafted Copolymers and the Respective Homopolymers.

Sample code	Segmental processes					Secondary processes	
	$\log[\tau_0^{\#}/\text{s}]^{\text{a}}$	B [K]	T_0 [K]	T_g [K] ^b	m^*	$\log[\tau_0/\text{s}]$	E_a [kJ·mol ⁻¹]
			α_{POEGMA}			β process	
POEGMA	-12	580 ± 40	195 ± 1	214 ± 1	149	-16.5 ± 0.6	57.0
PLMA ₁₆ - <i>b</i> -POEGMA ₈₄	-12	700 ± 50	187 ± 2	208 ± 2	143	-14.8 ± 0.3	50.1
PLMA ₅₂ - <i>b</i> -POEGMA ₄₈	-12	620 ± 60	192 ± 6	211 ± 6	157	-16.2 ± 0.7	55.6
PLMA	-	-	-	-	-	-12 ± 2	34.6
			α_{PLMA}			γ process	
POEGMA	-	-	-	-	-	-13.1 ± 0.3	31.9
PLMA ₁₆ - <i>b</i> -POEGMA ₈₄	-	-	-	-	-	-12.0 ± 0.3	28.2
PLMA ₅₂ - <i>b</i> -POEGMA ₄₈	-12	3200 ± 80	130 ± 4	229 ± 4	33	-14.1 ± 0.1	34.0
PLMA	-12	3060 ± 30	136 ± 1	231 ± 1	34	-13.2 ± 0.3	25.5

^a) held fixed; ^b) dielectric T_g obtained at $\tau = 100$ s.

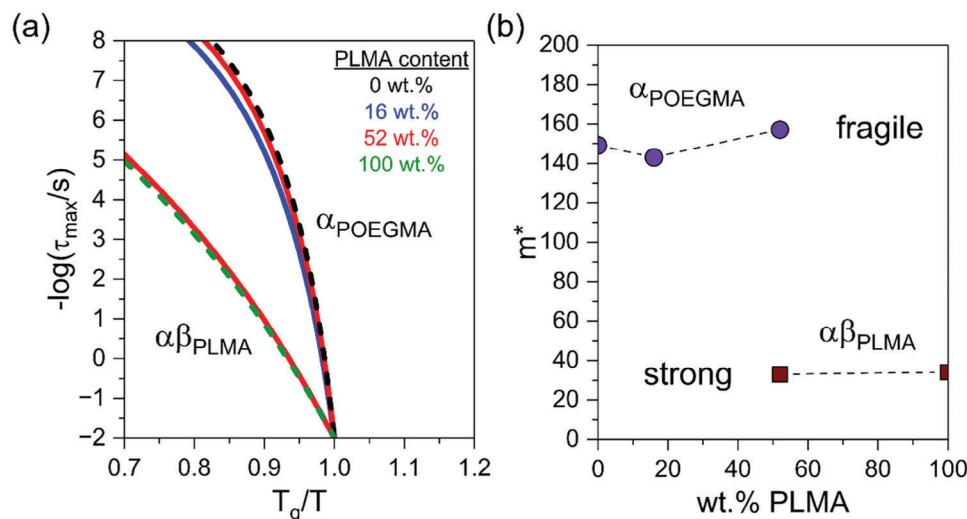


Figure 8. a) Relaxation times versus normalized temperature depicting the two segmental processes. b) Extracted values of fragility or steepness index as a function of PLMA composition, for the α_{POEGMA} (purple) and $\alpha\beta_{\text{PLMA}}$ (wine) processes.

ferent. The amphiphilic nature of the blocks induces nanophase segregation and gives rise to *heterogeneous dynamics*. Hence amphiphilicity drives the heterogeneous dynamics.

3.4. Ionic Conductivity

Dielectric spectroscopy enables the investigation of ionic mobility through the dc-conductivity. The latter in non-ionic systems arises from ionic impurities (such as minor amount of inorganic

salts in the monomers and solvents used in the synthesis) or the presence of protons (i.e., water molecules). The dc-conductivity is extracted from the plateau of the real part of complex conductivity, as illustrated in Figure S8 (Supporting Information). The temperature dependence of the extracted values are plotted as a function of reciprocal temperature in Figure 9a.

At ambient temperature, the dc-conductivity decreases by approximately five orders of magnitude in going from POEGMA to PLMA homopolymers, reflecting their differences in polarity. Similarly, the dc-conductivity of AmBCs decreases with the

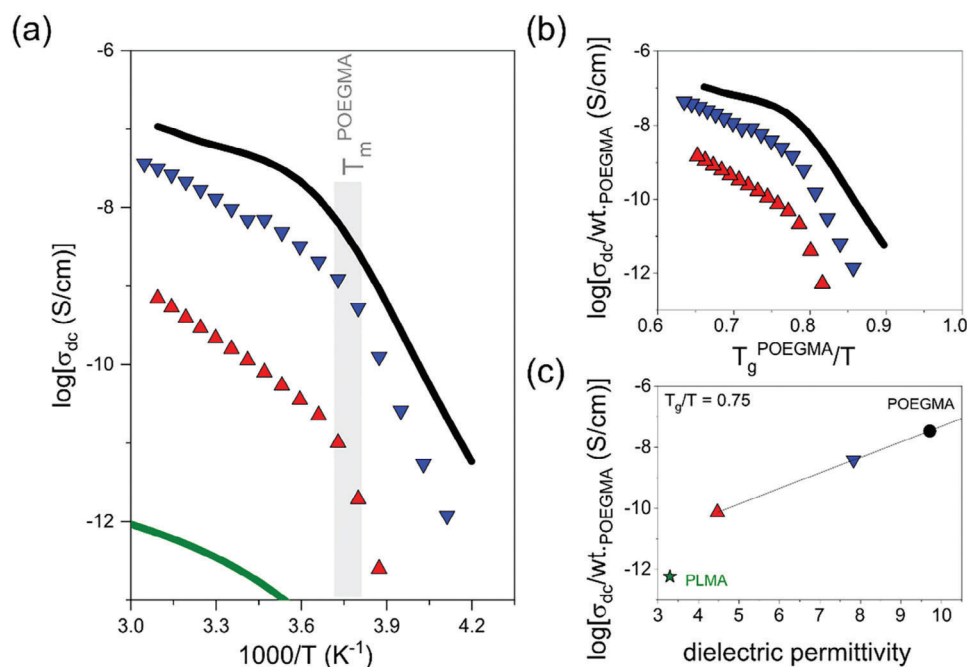


Figure 9. a) Temperature dependence of dc-conductivity for POEGMA (black line), PLMA_{16-b}-POEGMA₈₄ (blue down-triangles), PLMA_{52-b}-POEGMA₄₈ (red up-triangles), and PLMA (green line). b,c) Normalized conductivity with the weight fraction of the hydrophilic block and as a function of b) T_g^{POEGMA}/T and the measured c) dielectric permittivity.

reduction in POEGMA content. The dc-conductivity can be influenced by several factors: i) the POEGMA content and the associated dielectric permittivity, ii) the glass “transition” temperature T_g^{POEGMA} , and iv) the morphology.^[40] Figure 9b depicts the normalized conductivity values by the weight fraction of POEGMA as a function of reduced temperature by the T_g^{POEGMA} . Evidently, scaling of the measured conductivities by composition and by the POEGMA T_g does not suffice to explain ion conduction in the copolymers. Dielectric permittivity and morphology play an additional role. To this end, when compared at a fixed $T_g/T = 0.75$, the dc-conductivity increases with increasing dielectric permittivity (see Figure 9c). This is understandable, as increasing dielectric permittivity better facilitates ion dissociation. Contrast this with the PLMA homopolymer; the low permittivity value excludes ion dissociation that gives rise to the low conductivity values. Additionally, the bcc morphology is anticipated to enhance ion transport through its percolating network (i.e., 3D ionic paths), as compared to the lamellar nanostructure. The latter, depending on the lamellar orientation with respect to the electrodes could reduce, and in extreme cases even block, ion transport.

Overall, the investigated AmBCs exhibit strong immiscibility between the two blocks, leading to *nanophase separation* and *heterogeneous dynamics*, featuring distinct homopolymer-rich dynamics and confinement effects. Of key importance to these effects is the amphiphilic nature of the diblock copolymer.

4. Conclusion

In this study, we examined the nanophase separation and molecular dynamics of amphiphilic diblock copolymers with a densely grafted architecture, specifically focusing on PLMA-*b*-POEGMA copolymers containing 16 and 52 wt.% PLMA. SAXS results confirmed the strong segregation between the POEGMA and PLMA blocks, resulting in distinct nanodomains. The symmetric and asymmetric diblock copolymers exhibited lamellar and bicontinuous cubic phases, respectively. In addition, the asymmetric diblock copolymer displayed enhanced long-range order, attributed to its higher molar mass. The segregation strength between the two components and the presence of distinct POEGMA and PLMA nanodomains were corroborated by observing the (weak) crystallization/melting of POEGMA side chains through thermodynamics (DSC) and isochronal dielectric measurements. Molecular dynamics by DS revealed that the local segregation between the blocks leads to heterogeneous segmental dynamics, closely associated with those of the parent homopolymers. As a result, two glass temperatures (T_g s) were identified in the symmetric diblock copolymer using both dielectric and temperature-modulated DSC measurements. Additionally, confinement effects were evidenced for the low T_g component in the copolymers. Ionic conductivity in the diblocks – originating from impurities – was found to depend on the POEGMA content (through its high dielectric permittivity) and the copolymer morphology. The highest ion conductivity was found in the copolymer where POEGMA is the majority phase forming continuous ion paths. In the glassy state, the dielectric spectra were predominantly influenced by the local dynamics of POEGMA. Overall, this study provides insights into the effect of amphiphilicity on the self-assembly and dynamics of diblock copolymers with a densely grafted architecture.

Supporting Information

Supporting Information is available from the Wiley Online Library or from the author.

Acknowledgements

This research received no external funding.

Conflict of Interest

The authors declare no conflict of interest.

Data Availability Statement

The data that support the findings of this study are available from the corresponding author upon reasonable request.

Keywords

amphiphilic diblock copolymers, densely grafted architecture, molecular dynamics, nanophase separation

Received: June 8, 2024

Revised: July 10, 2024

Published online: August 16, 2024

- [1] N. Hadjichristidis, S. Pispas, G. Floudas, *Block Copolymers: Synthetic Strategies, Physical Properties, and Applications*, John Wiley & Sons, Hoboken, New Jersey 2003.
- [2] F. S. Bates, G. H. Fredrickson, *Physics Today* 1999, 52, 32.
- [3] A. Skandalis, S. Pispas, *J. Polym. Sci., Part A: Polym. Chem.* 2017, 55, 155.
- [4] A. Skandalis, A. Sergides, A. Bakandritsos, S. Pispas, *Polymers* 2017, 10, 14.
- [5] H. F. Mark, *Encyclopedia of Polymer Science and Technology, Concise*, John Wiley & Sons, Hoboken, New Jersey 2013.
- [6] Y. Mai, A. Eisenberg, *Chem. Soc. Rev.* 2012, 41, 5969.
- [7] S. Pispas, N. Hadjichristidis, *Langmuir* 2003, 19, 48.
- [8] A. Pipertzis, M. Kafetzi, D. Giaouzi, S. Pispas, G. A. Floudas, *ACS Appl Polym Mater* 2022, 4, 7070.
- [9] O. Vassiliadou, V. Chrysostomou, S. Pispas, P. A. Klonos, A. Kyritsis, *Soft Matter* 2021, 17, 1284.
- [10] G. Floudas, P. Placke, P. Štěpánek, W. Brown, G. Fytas, K. Ngai, *Macromolecules* 1995, 28, 6799.
- [11] G. Floudas, P. Štěpánek, *Macromolecules* 1998, 31, 6951.
- [12] P. Panagos, G. Floudas, *J. Non-Cryst. Solids* 2015, 407, 184.
- [13] A. Pipertzis, A. Hess, P. Weis, G. Papamokos, K. Koynov, S. Wu, G. Floudas, *ACS Macro Lett.* 2018, 7, 11.
- [14] M. Beiner, H. Huth, *Nat. Mat.* 2003, 2, 595.
- [15] F. Garwe, A. Schönhals, H. Lockwenz, M. Beiner, K. Schroter, E. Donth, *Macromolecules* 1996, 29, 247.
- [16] A. Karatza, P. Klonos, S. Pispas, A. Kyritsis, *Polymer* 2019, 181, 121794.
- [17] M. Mierzwa, G. Floudas, M. Neidhofer, R. Graf, H. W. Spiess, W. H. Meyer, G. Wegner, *J. Chem. Phys.* 2002, 117, 6289.
- [18] G. Moad, E. Rizzardo, S. H. Thang, *Aust. J. Chem.* 2006, 59, 669.
- [19] G. Moad, E. Rizzardo, S. H. Thang, *Polymer* 2008, 49, 1079.
- [20] A. Skandalis, T. Sentoukas, D. Selianitis, A. Balafouti, S. Pispas, *Materials* 2024, 17, 1947.

- [21] S. L. Simon, *Thermochim. Acta* **2001**, 374, 55.
- [22] B. Wunderlich, Y. Jin, A. Boller, *Thermochim. Acta* **1994**, 238, 277.
- [23] F. Kremer, A. Schönhal, *Broadband Dielectric Spectroscopy*, Springer Science & Business Media, Berlin, Germany **2002**.
- [24] G. Floudas, in *Polymer Science: A Comprehensive Reference*, (Eds: K. Matyjaszewski, M. Möller), Elsevier, Amsterdam **2012**, pp. 825–845.
- [25] S. Havriliak, S. Negami, *Polymer* **1967**, 8, 161.
- [26] Y. Shi, H. Schmalz, S. Agarwal, *Polym. Chem.* **2015**, 6, 6409.
- [27] A. Czaderna-Lekka, M. Kozanecki, M. Matusiak, S. Kadlubowski, *Polymer* **2021**, 212, 123247.
- [28] A. Aluculesei, A. Pipertzis, V. Piunova, G. Miyake, G. Floudas, G. Fytas, R. Grubbs, *Macromolecules* **2015**, 48, 4142.
- [29] T. P. Lodge, E. R. Wood, J. C. Haley, *J. Polym. Sci., Part B: Polym. Phys.* **2006**, 44, 756.
- [30] G. Adam, J. H. Gibbs, *J. Chem. Phys.* **1965**, 43, 139.
- [31] E. Donth, *J. Non-Cryst. Solids* **1982**, 53, 325.
- [32] A. Selevou, G. Papamokos, M. Steinhart, G. Floudas, *J. Phys. Chem. B* **2017**, 121, 7382.
- [33] J. Bartels, J. H. H. Wang, Q. Chen, J. Runt, R. H. Colby, *Macromolecules* **2016**, 49, 1903.
- [34] D. J. Kinning, E. L. Thomas, *Macromolecules* **1984**, 17, 1712.
- [35] X. Jin, S. Zhang, J. Runt, *Polymer* **2002**, 43, 6247.
- [36] G. Zardalidis, J. Mars, J. Allgaier, M. Mezger, D. Richter, G. Floudas, *Soft Matter* **2016**, 12, 8124.
- [37] K. Ngai, G. Floudas, D. Plazek, A. Rizos, *Encyclopedia of Polymer Science and Technology*, John Wiley & Sons, Hoboken, New Jersey **2002**.
- [38] M. Spyridakou, E. Iliopoulou, K. Peponaki, S. Alexandris, E. Filippidi, G. Floudas, *Macromolecules* **2023**, 56, 4336.
- [39] C. Grigoriadis, A. Nese, K. Matyjaszewski, T. Pakula, H.-J. Butt, G. Floudas, *Macromol. Chem. Phys.* **2012**, 213, 1311.
- [40] A. Pipertzis, G. Papamokos, M. Mühlhngaus, M. Mezger, U. Scherf, G. Floudas, *Macromolecules* **2020**, 53, 3535.